Asad, Bilal; Vaimann, Toomas; Belahcen, Anouar; Kallaste, Ants; Rassolkin, Anton; Khang, Huynh V.; Ghahfarokhi, Payam S.; Naseer, Muhammad U.; Iqbal, Muhammad N.

The modeling and investigation of slot skews and supply imbalance on the development of principal slotting harmonics in squirrel cage induction machines

Published in:
IEEE Access

DOI:
10.1109/ACCESS.2021.3134331

Published: 09/12/2021

Document Version
Publisher's PDF, also known as Version of record

IEEE Access
Multidisciplinary | Rapid Review | Open Access Journal

Received November 23, 2021, accepted December 6, 2021, date of publication December 10, 2021,
date of current version December 24, 2021.

Digital Object Identifier 10.1109/ACCESS.2021.3134331

The Modeling and Investigation of Slot Skews and Supply Imbalance on the Development of Principal Slotting Harmonics in Squirrel Cage Induction Machines

BILAL ASAD[1,2], (Member, IEEE), TOOMAS VAIMANN[1], (Senior Member, IEEE), ANOUAR BELAHCEN[2], (Senior Member, IEEE), ANTS KALLASTE[1], (Senior Member, IEEE), ANTON RASSOLKIN[1], (Senior Member, IEEE), HUYNH VAN KHANG[3], (Senior Member, IEEE), PAYAM SHAMS GHAHFAROKHI[1,4], (Member, IEEE), MUHAMMAD U. NASEER[1], (Member, IEEE), AND MUHAMMAD N. IQBAL[1], (Member, IEEE)

[1]Department of Electrical Power Engineering and Mechatronics, Tallinn University of Technology, 19086 Tallinn, Estonia
[2]Department of Electrical Engineering and Automation, Aalto University, 00076 Aalto, Finland
[3]Department of Engineering Sciences, Faculty of Engineering and Science, University of Agder, 4879 Grimstad, Norway
[4]Department of Electrical Machines and Apparatus, Riga Technical University, Riga LV-1658, Latvi

Corresponding author: Bilal Asad (bilal.asad@aalto.fi)

This work was supported by European Economic Area (EEA)/Norway Grants 2014–2021 (Industrial Internet Methods for Electrical Energy Conversion Systems Monitoring and Diagnostics).

ABSTRACT A discrete winding function analysis (DWFA) based approach for the modelling of skewed rotor cage-type induction motor with minimal simulation time is presented in this paper. The rotor slot skew has a significant attenuating impact on principal slotting harmonics (PSH) or rotor slotting harmonics (RSH). These harmonics can play a significant role in sensor-less speed estimation and condition monitoring of induction machines. The advanced fault diagnostic algorithms are becoming increasingly dependent on the fast and accurate mathematical models of electrical machines. The most accurate models are based on the finite element method (FEM), but the computational complexity and the required simulation time make them unsuitable for model-dependent fault diagnostic algorithms. Moreover, as most models are 2D, they cannot incorporate axial asymmetries such as rotor slot skews. Furthermore, most analytical models, such as modified winding function analysis (MWFA), depend upon the continuous integration functions, increasing complexity while implementing them in the online environment in digital signal processing boards. To resolve all those issues, DWFA based model is proposed in this paper, which can simulate the majority of the faults in negligible time compared to the corresponding FEM models. The impact of slot skews and unbalanced power supply on the current spatial harmonics is studied, and the results are compared with the practical measurements taken from the laboratory setup.

INDEX TERMS Analytical models, discrete-time systems, condition monitoring, electrical machines, electromagnetic modeling, fault diagnosis, induction motors.

I. INTRODUCTION

The role of induction machines in modern-day society is indispensable because of their simple and rugged structure, low cost, easy maintenance and reliability. Their dominant and frequent use increases the importance of their mathematical models not only for design and control but also for their condition monitoring. As the faults in electrical machines are degenerative, their detection at the embryonic stage is of crucial importance to avoid any catastrophic situation. Varieties of very mature diagnostic algorithms, which do not depend upon the model of the system, are available in the

The associate editor coordinating the review of this manuscript and approving it for publication was Dazhong Ma.

literature. However, with the increasing trend of industrial inverters, conventional diagnostic algorithms such as MCSA do not remain straightforward. Moreover, those techniques may also vary according to the motor working environment. The common diagnostic techniques that do not depend upon the motor model are MCSA, thermal analysis, acoustic analysis, stray flux monitoring, partial discharge analysis, air gap flux monitoring etc. [1].

The conventional diagnostic techniques related problems can be avoided by using advanced model-dependent condition monitoring techniques. The reliable model-based diagnostic algorithms depend upon the accurate and fast mathematical models of induction motors. These models can be used for the fault identification and severity estimation [2], [3], for the training of multi-agent systems [4], for the development of vector classifiers [5, for the comparison of fault indexes [6], for online parameters estimation [7], [8], and motor drives [9, etc. Among several model-dependent condition monitoring techniques, the artificial intelligence (AI) based fault diagnostic techniques are gaining heightened popularity [10]. The only challenge with AI techniques is the requirement of big data for training purposes. The training data set should have as many healthy and faulty cases as possible for better reliability of the diagnostic algorithm.

The collection of big data with all possible faulty cases is very challenging from the industry as well as from the laboratory environments. From industry, it is difficult because of the limited number of faulty machines working due to preventive maintenance. Moreover, the training data set should have signals with very well-defined types and severity of the fault so that they can be considered as benchmark signals. On the other hand, from the laboratory, it is difficult as a limited number of destructive tests can be performed due to economic limitations.

The only possible solution is the mathematical model that can simulate various faults within an acceptable duration of time. The mathematical models can be broadly classified into two categories: Analytical and Numerical. A typical example of numerical models is the finite element method (FEM) based models. The FEM based models can give promising results as almost all practical aspects can be included [11]–[13], making them suitable for design problems. Those aspects can be related to material, geometry and winding configuration. The only problem with FEM modeling is the amount of simulation time that is not feasible for fault diagnostic algorithms. These models cannot easily become the part of drive because of associated limited computational resources. Moreover, these models are not feasible for inverse problem theory where observables are mapped towards the unknowns. The reason for this is the FEM solution related large matrices whose inverse solution cannot give stable and unique results. The most common example of analytical models is the magnetic circuit coupling (MCC) based models. In these models, the electrical circuit's equations are used for the simulation of performance parameters. The most common MCC models are the winding function analysis (WFA) based models where machine design parameters can be defined with the help of Fourier summation or conditional analytical equations.

Considerable work has already been reported in this domain. For example, The authors of [14] simulated stator short circuit faults in squirrel cage induction motor (SQIM) using winding function analysis (WFA) while the broken rotor bars were presented in [15]. The authors of [16] used this approach to analyze various faults, such as stator phase disconnection, broken bars, and broken end rings. The WFA approach for the analysis of adjustable speed drive applications is presented in [17], [18]. The modelling of a permanent magnet machine with a fractional slot concentrated winding can be studied in [19]. In most of the WFA based models, the air gap is considered constant, making the model unsuitable for implementing eccentricity-based faults. Moreover, the effects of stator and rotor slot openings cannot be studied. These studies may also include the effects of general and local saturations. Furthermore, these models are unsuitable for sensor-less speed drive systems as the principal slotting harmonics (PSH) are potentially ignored.

These problems can be solved using the modified winding function analysis (MWFA) method, where the slot openings of the stator and rotor can be considered by making the air gap a function of the stator and rotor relative position. The authors in [20] extended the WFA based method to simulate electrical machines with a non-uniform air gap. The use of the MWFA to model the stator and rotor slot effects for speed sensor-less drive systems is presented in [21]. The static and dynamic eccentricities are presented in [22] and [23], respectively. Unlike [21], where the air gap permeance is approximated by cosine series functions, [24] used the actual stator and rotor slot opening functions and a medium magnetic equipotential surface to simulate the machine. By doing so, the authors obtained results very close to the ones obtained from FEM. The simulation time was further reduced by exploiting the symmetry of the rotor cage, however, it is not valid in the case of faulty machines. The primary approximation frequently used in all the papers cited earlier is that; the machine is symmetrical in the axial direction, which is not always true. In most machines, the rotor slots are skewed to attenuate the rotor slotting harmonics (RSH). Those harmonics are attenuated for the reduction of speed and torque ripples. In this paper, a novel technique for implementing rotor skews is proposed. In continuation of [25], this paper has the following attractive features.

- Unlike most of the papers where an integral function is solved for the calculation of inductances, in this research, a discrete mean value equation is proposed. The derived mean value equation reduces the computational complexity and the integral calculation-based approximations.
- The proposed DWFA formula is further extended to incorporate the machine's axial asymmetries such as rotor slots skew.

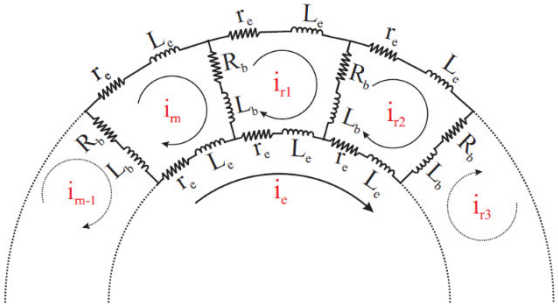

FIGURE 1. The equivalent circuit diagram of rotor cage.

- Unlike most of the papers where the spatial harmonics are defined with the help of Fourier summation of the selective number of harmonics, in this paper the winding functions and the air gap is defined with the help of conditional analytical expressions. The approximations related to the self-defined number of harmonics and their amplitude can be avoided by doing so.
- The impact of rotor slot skews on PSH amplitude is studied, while in most of the papers, it is neglected.
- The impact of negative sequence currents on the development of spatial harmonics is investigated.
- The model is divided into online and offline portions. All the inductances are calculated in the offline portion, and the results are saved in 3-D lookup tables. Once the offline calculation is done, most of the faults can be simulated in the online portion without doing unnecessary offline calculations again.

II. THE ANALYTICAL MODEL

The induction machines are magnetically coupled electrical circuits. Mostly the primary windings are static and associated with the stator side, while secondary windings are associated with the rotor and rotate with it. The magnetic coupled circuits theory-based voltage equations of a squirrel cage induction motor are described as;

$$\boldsymbol{V}_s = \boldsymbol{I}_s\boldsymbol{R}_s + \frac{d}{dt}\boldsymbol{\varphi}_s, \tag{1}$$

$$\boldsymbol{0} = \boldsymbol{I}_r\boldsymbol{R}_r + \frac{d}{dt}\boldsymbol{\varphi}_r, \tag{2}$$

where **V**s, **I**s, **I**r, **R**s and **R**r are vectors containing stator three-phase voltage, stator three-phase current, stator resistances, and rotor resistances. While φs and φr are the stator and rotor fluxes, respectively. The voltage matrix on the rotor side is zero because the end rings are short-circuiting the rotor phases that are bars in cage-induction machines.

The following equations present the detailed description of voltage equations of stator and rotor in the form of matrices that makes the implementation of the model easier (3) and (4), as shown at the bottom of the next page.

The matrix elements with subscript "s" and "r" are respective stator and rotor associated entries. The dimension of rotor related matrices depends upon the number of bars in it plus one more which corresponds to the end ring. The end ring-related rows and columns shown in (4) could be neglected because their value is minimal and the end ring current is approximately zero because all rotor phases are equally mechanically spaced. Nevertheless, neglecting them can cause the problems of singularities while taking the inverse of matrices, and the end ring faults cannot be implemented. The equivalent circuit diagram of the rotor cage is shown in Figure (1), from where (4) can be written using simple voltage equations.

The stator flux is the function of stator self and mutual inductances and their corresponding currents (5).

$$\boldsymbol{\varphi}_s = \boldsymbol{L}_{ss}\boldsymbol{I}_s + \boldsymbol{L}_{sr}\boldsymbol{I}_r, \tag{5}$$

where $\boldsymbol{L}_{ss}$ and $\boldsymbol{L}_{sr}$ are matrices containing stator and rotor self and mutual inductances, as presented below:

$$\boldsymbol{L}_{ss} = \begin{bmatrix} L_{aas} & L_{abs} & L_{acs} \\ L_{bas} & L_{bbs} & L_{bcs} \\ L_{cas} & L_{cbs} & L_{ccs} \end{bmatrix},$$

$$\boldsymbol{L}_{sr} = \begin{bmatrix} L_{ar1} & L_{ar2} & \dots & L_{ari} & \dots & L_{arn} & L_{are} \\ L_{br1} & L_{br2} & \dots & L_{bri} & \dots & L_{brn} & L_{bre} \\ L_{cr1} & L_{cr2} & \dots & L_{cri} & \dots & L_{crn} & L_{cre} \end{bmatrix},$$

$$\boldsymbol{L}_{sr} = \begin{bmatrix} L_{ar1} & L_{ar2} & \dots & L_{ari} & \dots & L_{arn} & 0 \\ L_{br1} & L_{br2} & \dots & L_{bri} & \dots & L_{brn} & 0 \\ L_{cr1} & L_{cr2} & \dots & L_{cri} & \dots & L_{crn} & 0 \end{bmatrix},$$

The subscripts a,b,c, and r represent entries related to the stator and rotor phases.

Similarly, rotor fluxes can be represented as:

$$\boldsymbol{\varphi}_r = \boldsymbol{L}_{rs}\boldsymbol{I}_s + \boldsymbol{L}_{rr}\boldsymbol{I}_r = \boldsymbol{L}_{sr}^T\boldsymbol{I}_s + \boldsymbol{L}_{rr}\boldsymbol{I}_r, \tag{6}$$

$$L_{rr} = \begin{bmatrix} L_{r1r1} & L_{r1r2} & \cdots & L_{r1ri} & \cdots & L_{r1rn} & L_{r1re} \\ L_{r2r1} & L_{r2r2} & \cdots & L_{r2ri} & \cdots & L_{r2rn} & L_{r2re} \\ \vdots & \vdots & \vdots & \vdots & \vdots & \vdots & \vdots \\ L_{rir1} & L_{rir2} & \cdots & L_{riri} & \cdots & L_{rirn} & L_{rire} \\ \vdots & \vdots & \vdots & \vdots & \vdots & \vdots & \vdots \\ L_{rnr1} & L_{rnr2} & \cdots & L_{rnri} & \cdots & L_{rnrn} & L_{rnre} \\ L_{rer1} & L_{rer2} & \cdots & L_{reri} & \cdots & L_{rern} & L_{rere} \end{bmatrix}$$

The rotor end-ring leakage inductance depends upon the number of rotor phases (n_b), the number of stator phases (m), the number of pole pairs (P), the bar length (l_{bar}), stator effective length (l_s), a factor (v = 0.18 for P > 1) and the average ring diameter (D_r) as in (7) [24].

$$L_e = \mu_o \frac{n_b}{3mP^2}\left((l_{bar} - l_s) + v\frac{\pi D_r}{2P}\right), \tag{7}$$

III. THE FORMATION OF DWFA METHOD AND INCORPORATING ROTOR SKEW

Other than the leakage, various magnetization inductances in induction machines can be classified as; stator-stator self, stator-stator mutual, stator-rotor mutual, rotor-rotor self and rotor-rotor mutual inductances. The main contributing factors among many for these inductances are stator and rotor winding configurations, air gap permeance functions, radius,

and the machine's length. According to the winding function based theory, those inductances can be calculated using (8).

$$L_{ij}(\theta e) = \mu_o rl \int_0^{p\pi} \mathrm{P}(\theta e, \alpha) N_i(\theta e, \alpha) n_j(\theta e, \alpha) d\theta e, \quad (8)$$

where μ_o is the permeability of the free space, r is the mid-air-gap radius of the machine, l is the effective length of the machine, $\mathrm{P}(\theta_e, \alpha)$ is the inverse air gap permeance function, $\mathrm{N}(\theta_e, \alpha)$ is the winding function, and $\mathrm{n}(\theta_e, \alpha)$ is the turn function. The theta (θ_e) and alpha (α) are the rotor and stator angles from a fixed reference point. These angles can be electrical or mechanical and will be equal in the case of a two-pole machine.

The integrator shows the summation of all rotor position-dependent variables multiplied at each position in the continuous-time domain. The usual integration calculation is based on the area under the curve, which can be calculated using the trapezoidal rule. Unfortunately, this rule not only increases the error but also increases the complexity of the integral solution. To avoid those problems, (8) can be reduced to a mean value function, as shown by (9).

$$L_{ij}(\theta e) = p\pi\mu_o l < r_g((\theta e, \alpha)\mathrm{P}((\theta e, \alpha) N_i((\theta e, \alpha) n_j((\theta e, \alpha) >, \quad (9)$$

Since all the inductances are supposed to be calculated at different rotor positions from 0 to 2π mechanical, the problem is no longer in the continuous-time domain. Instead, it can be considered in a discrete-time domain where all rotor position-dependent functions can be defined as vectors having "n" elements. Then, all those vectors can be multiplied in an element-wise manner. Finally, the average can be calculated by adding the elements of the resultant vector and dividing it by the total number of steps as shown by (10). By doing so, the integral complexity with the increasing number of rotor position-dependent variables does not remain a problem anymore. Moreover, the exploitation of constant air gap and complex analytical representation of various inductances as in [26], [27] can be easily avoided.

$$L_{ij}(\theta e) = \frac{p\pi\mu_o l}{n} \times \sum_{k=1}^{n} \left(r_g((\theta e, \alpha)\mathrm{P}((\theta e, \alpha) N_i((\theta e, \alpha) n_j((\theta e, \alpha))\right)_k \quad (10)$$

where the element-wise multiplication of all rotor position-dependent variables will create a vector of "n" elements. All elements are then added and divided by "n" to get the mean value.

Till this point, the machine is in two dimensions (x, y) while the third axial dimension is neglected. Usually, the induction machines in the axial direction are considered symmetrical, which is not always true. The most common reason for axial asymmetry is the stator and rotor slot skews, which reduce speed and torque ripples.

The rotor slot skews can be included by introducing a third angle known as skew angle (α_{sk}). The rotor can be divided into "n" number of segments in the axial direction, and the inductances of all segments can be calculated separately. Since all segments are serially attached, the final inductance vector will be equal to the sum of all individual segment vectors, as shown by (11) and (12).

$$L_{ij}(\theta e) = \frac{p\pi\mu_o}{n} \times \left[l_1 \sum_{k=1}^{n} \left(r_{g1}((\theta e, \alpha) P_1((\theta e, \alpha) N_{i1}((\theta e, \alpha) n_{j1}((\theta e, \alpha)\right)_k$$

$$\begin{bmatrix} v_{as} \\ v_{bs} \\ v_{cs} \end{bmatrix} = \begin{bmatrix} R_{as} & 0 & 0 \\ 0 & R_{bs} & 0 \\ 0 & 0 & R_{cs} \end{bmatrix} \begin{bmatrix} i_{as} \\ i_{bs} \\ i_{cs} \end{bmatrix} + \frac{d}{dt} \begin{bmatrix} \varphi_{as} \\ \varphi_{bs} \\ \varphi_{cs} \end{bmatrix}, \quad (3)$$

$$\begin{bmatrix} 0 \\ 0 \\ \vdots \\ 0 \\ 0 \\ 0 \end{bmatrix} = \begin{bmatrix} 2(R_b + r_e) & -R_b & 0 & 0 & \dots & 0 & -R_b & -r_e \\ -R_b & 2(R_b + r_e) & -R_b & 0 & \dots & 0 & 0 & -r_e \\ 0 & -R_b & 2(R_b + r_e) & -R_b & \dots & 0 & 0 & -r_e \\ \vdots & \vdots & \vdots & \vdots & \vdots & \vdots & \vdots & \vdots \\ 0 & 0 & 0 & 0 & \dots & 2(R_b + r_e) & -R_b & -r_e \\ -R_b & & 0 & 0 & \dots & -R_b & 2(R_b + r_e) & -r_e \\ -r_e & -r_e & -r_e & -r_e & \dots & -r_e & -r_e & n_b re \end{bmatrix} * \begin{bmatrix} i_{r1} \\ i_{r2} \\ i_{r3} \\ \vdots \\ i_{r(n-1)} \\ i_{rn} \\ i_{re} \end{bmatrix} + \frac{d}{dt} \begin{bmatrix} \varphi_{r1} \\ \varphi_{r2} \\ \varphi_{r3} \\ \vdots \\ \varphi_{r(n-1)} \\ \varphi_{rn} \\ \varphi_{re} \end{bmatrix} \quad (4)$$

$$+ l_2 \sum_{k=1}^{n} \left(r_{g2}((\theta e, \alpha) P_2((\theta e, \alpha) N_{i2}((\theta e, \alpha) n_{j2}((\theta e, \alpha)) \right)_k + \cdots + l_n \sum_{k=1}^{n} \left(r_{gn}((\theta e, \alpha) P_n((\theta e, \alpha) N_{in}((\theta e, \alpha) n_{jn}((\theta e, \alpha)) \right)_k \Bigg] \tag{11}$$

$$L_{ij}(\theta e) = \frac{p\pi\mu_o}{n} \times \sum_{s=1}^{n} \sum_{k=1}^{n} \left[l_s \begin{pmatrix} r_{gs}((\theta e, \alpha, \alpha_{sk}) \times P_s((\theta e, \alpha, \alpha_{sk}) \\ \times N_{is}((\theta e, \alpha, \alpha_{sk}) \times n_{js}((\theta e, \alpha, \alpha_{sk}) \end{pmatrix} \right]_k \tag{12}$$

All rotor position-dependent variables can be defined by shifting the corresponding reference vector by n elements for each segment. The number of shifting elements depends upon the number of segments and the samples per segment, as shown by (13) and (14).

$$l_{seg} = \frac{l_{ef}}{n_{seg}} \tag{13}$$

$$samples_{seg} = \frac{(sampes\ per\ skew\ angle\ in\ terms\ of\ stator\ slots)}{n_{seg}}$$
$$\alpha_{sk} = \text{skew angle} = n\ stator\ slot\ pitch \tag{14}$$

where l_{seg} is the segment length, l_{ef} is the rotor effective length, n_{seg} are the total number of segments in the axial direction.

All these inductances are saved in 3D tables as a function of rotor position. To calculate the machine performance parameters such as currents, fluxes, torque and speed, the pre-saved matrices are called as a function of rotor position. In the online simulation environment, the rotor position shall be used to index the corresponding 2D matrix. The main equations for the simulation of the machine's global variables are shown in (15) and (16).

$$T_e = \frac{1}{2}\left(\frac{p}{2}\right)\left(\boldsymbol{I}_r^T \frac{d}{d\theta}\boldsymbol{L}_{rs}\boldsymbol{I}_s + \boldsymbol{I}_s^T \frac{d}{d\theta}\boldsymbol{L}_{sr}\boldsymbol{I}_r\right), \tag{15}$$

$$J\frac{d}{dt}\omega_m = T_e - T_L - B_f\omega_m, \tag{16}$$

IV. THE PSH GENERATION CRITERIA

The leading causes of high-frequency current harmonics are the changing air gap and the non-sinusoidal distributed stator and rotor winding functions. Due to these factors, the air gap MMF distribution does not remain perfectly sinusoidal but becomes the function of the rotor position. These frequency components always remain present in the frequency spectrum of any healthy induction machine and yield speed and torque ripples. However, their amplitude can be attenuated by using an appropriate winding distribution on the stator side and putting a skewed cage on the rotor side. The eccentricity and principal slotting harmonics (PSH) or rotor slotting harmonics (RSH) in a squirrel cage induction machine can be described by the following equation;

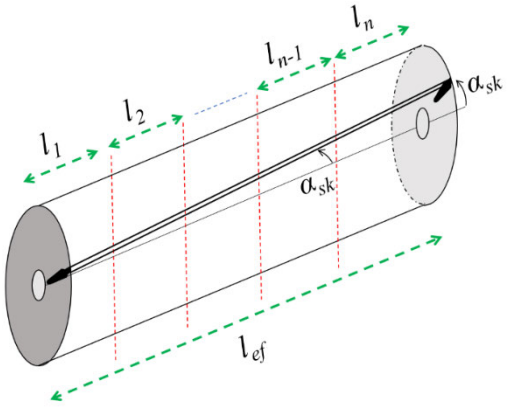

FIGURE 2. The description of rotor skew angle.

$$f_{ecce} = \left[(kn_b \pm n_d)\left(\frac{1-s}{P}\right) \pm v \right] fs, \tag{17}$$

And the mixed eccentricity by:

$$f_{ecce} = f_s \pm kf_r, \quad k = 1, 2, 3, \ldots \tag{18}$$

where n_d is the dynamic eccentricity which is 0 for static and 1, 2, 3, ... for dynamic eccentricity. n_b is the number of rotor bars, s is the slip, P is the number of pole pairs, k is any positive integer, v is the power supply based harmonic order, and f_s is the fundamental supply frequency.

Not all combinations of n_b and P can produce PSH in the current and voltage spectrum. The air gap MMF based harmonics, also known as PSH or RSH, will develop in stator voltage and current if any element from the set of P(6m ± 1) is equal to the stator winding based pole pair number of the space harmonics defined by $(Q - N_b - Pn)$ or $(Q - N_b + Pn)$ [21].

More precisely, the PSH or RSH will develop in the frequency spectrum if the following equality holds [28].

$$n_b = 2P\,[3\,(m \pm q) \pm r] \tag{19}$$

where m ± q = 0, 1, 2, 3 . . . and r = 0 or 1.

Out of two fundamental PSH components, one is more significant than the other. The most significant or PSH1 depends upon the winding distributions or air gap MMF distribution. The least significant component (PSH2) is due to the reverse rotating field because of the negative sequence currents. Even if PSH2 is absent in the simulation results, or the machine is not a PSH machine, the voltage imbalance and constructional imperfections can generate them in the healthy practical machine. Moreover, the changing air gap due to the stator and rotor slot openings also contribute to the production of PSH2. The following is the list of crucial factors that can have a direct influence on the presence and the amplitude of PSH components;

- Stator and rotor MMF
- Slot permeance functions
- Material saturation (flux fringing, rotor bridges)

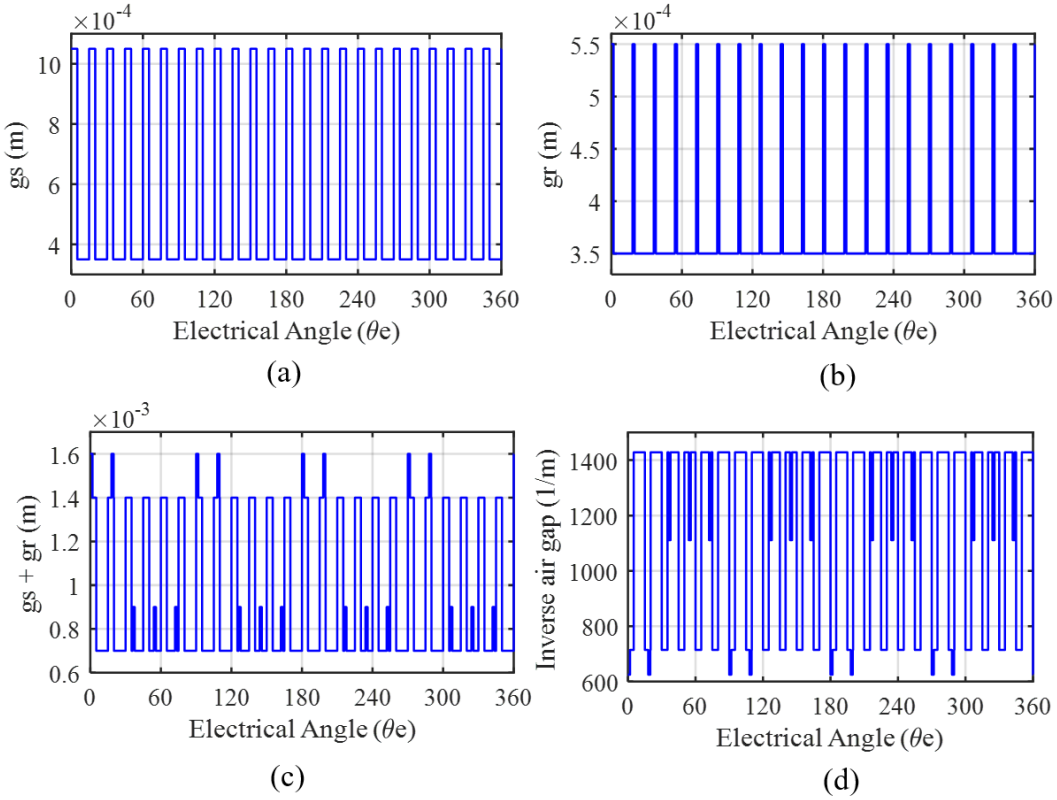

FIGURE 3. The air gap function of (a) the stator (gs), (b) the rotor (gr), (c) the net equivalent (gs+gr), and (d) the inverse air gap function at a specific rotor position.

- Slots skew
- Machine asymmetry (inherent eccentricity, unbalanced stator windings etc.)
- Unbalanced supply voltages

V. THE AIR-GAP AND WINDING FUNCTIONS

$$g_s(\theta e) = \begin{cases} r_g + h_{11}, & 0 \le \theta e \le B_{11} \\ r_g, & B_{11} < \theta e \le (B_{11} + B_{tt}), \end{cases} \quad (20)$$

$$g_r(\theta e, \alpha) = \begin{cases} r_g + h_{21}, & 0 \le \theta e \le B_{21} \\ r_g, & B_{21} < \theta e \le (B_{11} + B_{rt}), \end{cases} \quad (21)$$

The stator and rotor slot openings are the main reasons of the non-uniform air gap. From the air gap mid-point, the stator g_s (θe) and rotor g_r (θe, α) associated air gaps with the inclusion of slot openings can be defined using conditional analytical expressions.

Where B_{11}, B_{tt}, B_{21}, B_{rt}, h_{11}, h_{21}, r_g are the width (in terms of angle) of the stator slot opening, stator tooth tip, rotor slot opening, rotor tooth tip, stator slot depth without winding, the rotor bar depth, and the height of air gap centre respectively. The geometrical description of the stator and rotor slots can be found in [25].

The total air gap is the sum of both air gaps and changes with moving rotor, as shown in Figure (3). The extended lines in the total and the inverse air gaps are the locations where stator and rotor slot openings coincide with each other.

Similarly, the stator and rotor winding functions can be defined. Again, the stator winding function is stepped distributed, and on the rotor side, each pair of subsequent rotor bars represent each rotor phase, as shown in Figure (4).

VI. SIMULATION RESULTS

Each rotor segment produces the inductance profile similar to the adjacent segment but shifted by a specific number of samples described in equation (14).

The number of samples depends upon the number of samples per segment. Moreover, the number of shifted copies of the inductance profile depends upon the number of rotor segments. Figure 5 (a) shows the stator-rotor mutual inductance as the function of rotor position while the entire rotor is divided into four equally spaced segments. All shifted copied of the inductance profile will remain within the skew angle equal to one stator slot pitch in the motor under investigation. Since all segments are axially connected, the total inductance will be equal to the sum of all individual vectors. The final inductance profile tends to become smooth as the skew angle is introduced, as shown in Figure 5 (b). Figure 5 (a)-(b) intends to describe slot-related ripples' attenuation in the inductance profile as the skewed bar is considered. However, the length is taken as constant in all cases until this point for ease of understanding.

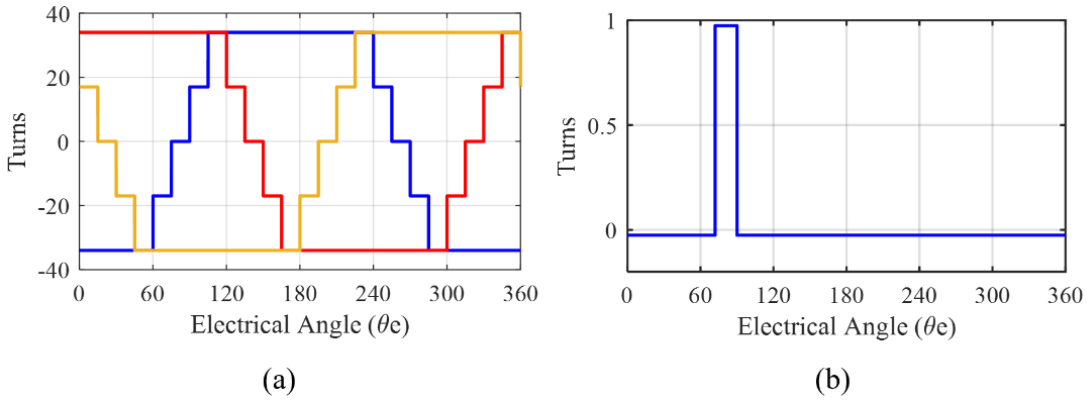

FIGURE 4. The winding functions (a) a three-phase stator, (b) one loop of the rotor.

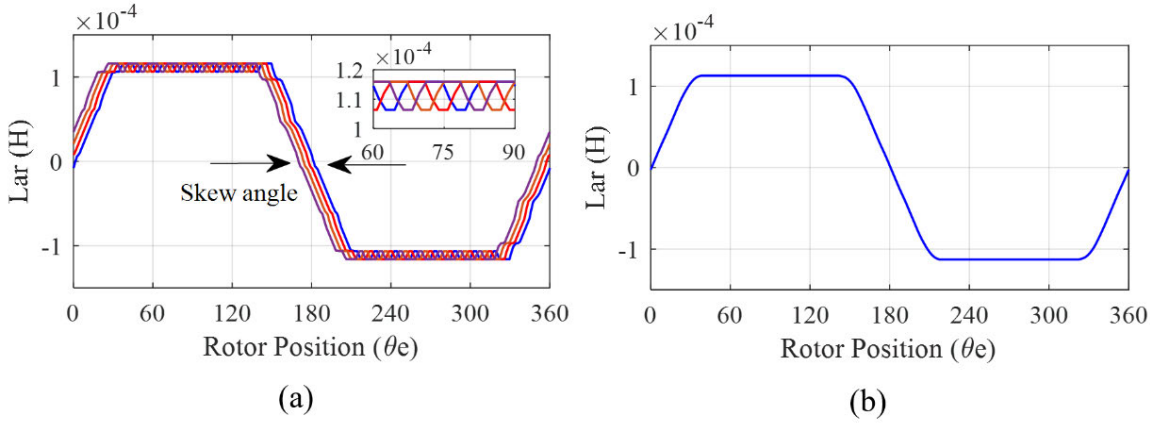

FIGURE 5. The stator-rotor mutual inductance, (a) for each segment (4 segments), (b) the final inductance.

Figure (6) shows the smoothing of all inductances with the inclusion of rotor slot skew. For comparison, the rotor is initially considered as a single piece without any skew. Then the rotor core is axially divided into forty equal segments with slot skew angle equal to one stator slot pitch. The blue line shows the inductance behaviour with the stepping rotor by considering it as non-skewed. The red lines show the smoothing of the inductance profiles when the skew is considered. The inductance profiles not only increases the smoothness but also reduce the peak-to-peak ripple magnitude. Since the machine has 48 stator slots, 40 rotor slots and 4 poles, the number of cycles of changing inductance till 120 degrees electrical angle are 8 on rotor-rotor and about 6.67 on stator-stator related inductances. However, the total number of cycles is 40 in stator related while 48 in rotor related inductances. The design parameters, such as winding functions and air-gaps, are defined by the vectors, each having a size equal to 10 × Qs × nb (19200). The vector size equal to the integral multiple of the number of stator and rotor slots avoids the problems of fractional number while implementing the equations. The rotor step size is equal to one sample, which corresponds to 0.0375 degrees electrical, giving better resolution.

The corresponding derivatives are shown in Figure (7), where it is evident that the rate of change of inductances with respect to the rotor position decreases significantly with the inclusion of rotor slot skew. The rate of changing inductances can be further reduced by increasing the skew angle.

The simulated phase currents with non-skewed and skewed rotor bars are shown in Figure (8) (a) and (b), respectively. In both cases, the pre-saved inductance matrices are used in an online environment. The simulation is performed with 19200 rotor steps equal to ten times the number of stator and rotor slots. As already discussed, the selection of an appropriate number of rotor steps is very crucial for simulation without any error. The number of rotor steps should be such that; it is divisible with the number of stator slots; it is divisible with the number of rotor bars—otherwise, any fractional value while calculating samples per slot pitch will lead to an error. Moreover, the number of rotor segments should equally divide the number of samples corresponding to the skew angle. All these conditions can be achieved by considering the rotor steps equal to "k" times the number of stator and rotor slots (21). The rotor slot skew based reduction in torque ripples is shown in Figures (8) (c) and (d). While for better comparison both skewed and non-skewed rotor based

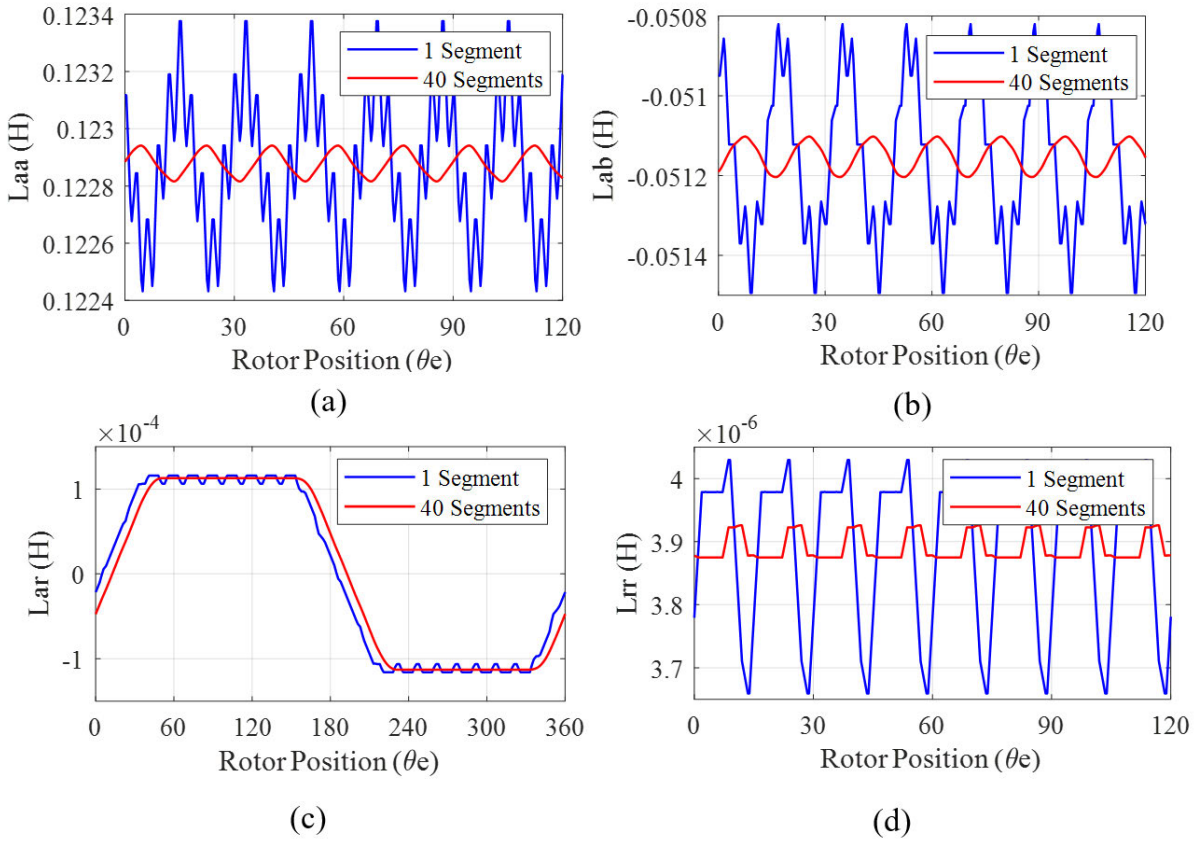

FIGURE 6. The calculated inductances with (red) and without (blue) rotor slots skew, (a) stator to stator self (Laa), (b) stator to stator mutual (Lab), (c) stator to the rotor (Lar), and (d) rotor to rotor (Lrr) concerning the rotor position.

torque profiles are shifted across the zero line.

$$f_s = k \times Q_s \times n_b; \quad k = 1, 2, 3, \ldots. \tag{22}$$

The simulated currents are much smoother with a skewed rotor than the corresponding rotor with non-skewed rotor bars. It is due to the attenuation of the PSH harmonics, as shown in Figure (9). In the machine under investigation with 40 rotor bars, two pole pairs, zero dynamic eccentricity, and 0.0067 slip, the PSH1 and PSH2 components will develop at 883 Hz and 983 Hz theoretically according to the equation (17). The machine is a PSH machine as it holds the equality given by equation (19). Both harmonics are attenuated from 0.04922 A and 0.0617 A to 0.00398 A and 0.00914 A, respectively while the same Hamming window is used for all cases.

Although, the skew angle attenuates the PSH components quite significantly. It should be appropriately optimized as, on the one hand, it attenuates the high-frequency components, but on the other hand, it decreases the machine power. Table 1 shows the impact of rotor bar skews in terms of stator slot pitch. It is clear that with the increase in the slot skew, the amplitude of PSH components decreases but slip increases with constant load. Similarly, the mean generated torque reduces under constant slip conditions. Therefore, the best practice is to make skew angle equal to one stator slot pitch as it is in the machine under investigation.

TABLE 1. The effect of slot skew on slip and generated torque.

Skew angle/slot pitch	RSH1 (Hz)	RSH2 (Hz)	Mean torque (N-m) for S=0.0667	Slip for the load (125N-m)
0	0.04249	0.06170	121.56	0.0667
1	0.00398	0.00914	119.95	0.0691
2	0.00215	0.00727	113.50	0.0752
3	0.00204	0.00625	99.55	0.1342
4	0.00142	0.00460	81.07	unstable

TABLE 2. The development of PSH with skewed rotor.

Simulation slip	RSH1 (Hz)	RSH2 (Hz)	RSH1 (A)	RSH2 (A)
0.0030	946.96	1047	0.00047	0.0005
0.035	914.90	1015	0.00231	0.0048
0.05	899.90	1000	0.00332	0.0068
0.0667	883.17	983.27	0.00454	0.0075

It is worth mentioning here that the current spectrum in Figures 9 and 10 are of phase current that is why both PSH1 and PSH2 components are visible. However, in the case of a perfectly symmetrical machine with a balanced supply PSH2 component will disappear from the line current.

As described by equation (17), the slotting harmonics are the function of slip in terms of frequency and amplitude. Figure (10) shows the movement of these components as the slip increases from 0.0030 to 0.05. The skew in

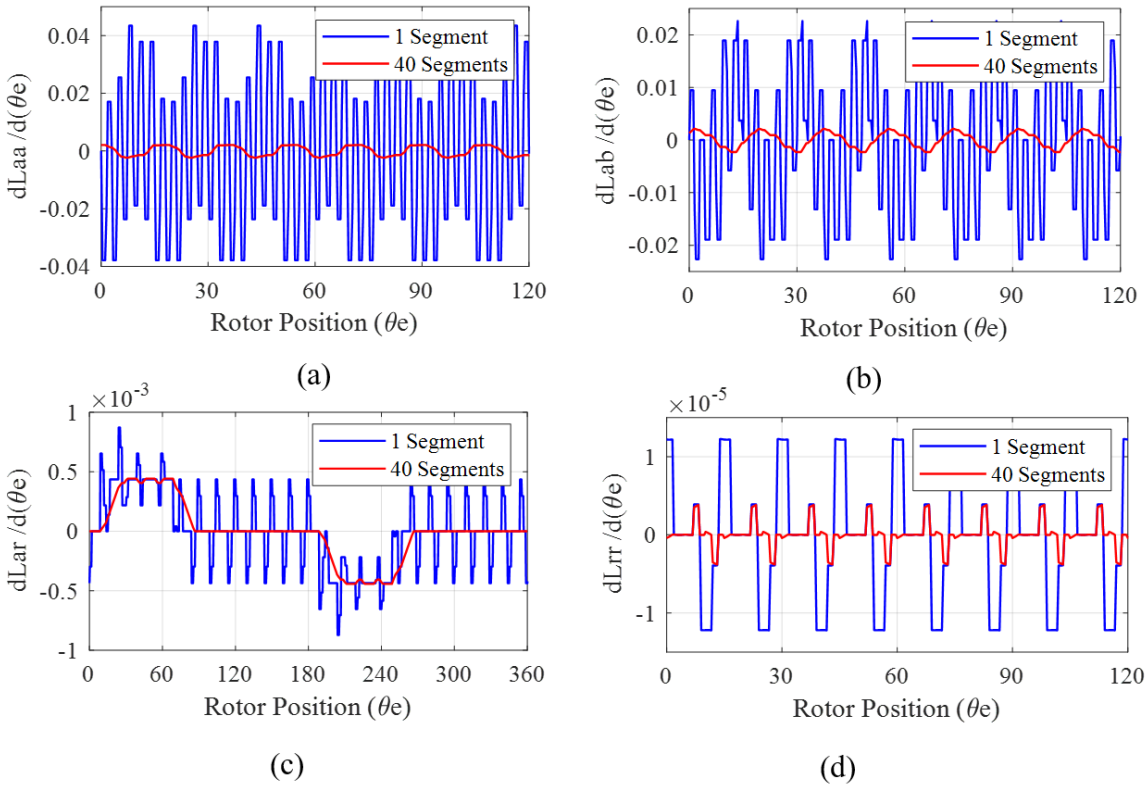

FIGURE 7. The derivative of the inductances with (red) and without (blue) rotor slot skews (a) stator to stator self (Laa), (b) stator to stator mutual (Lab), (c) stator to the rotor (Lar), and (d) rotor to rotor (Lrr) with respect to the rotor position.

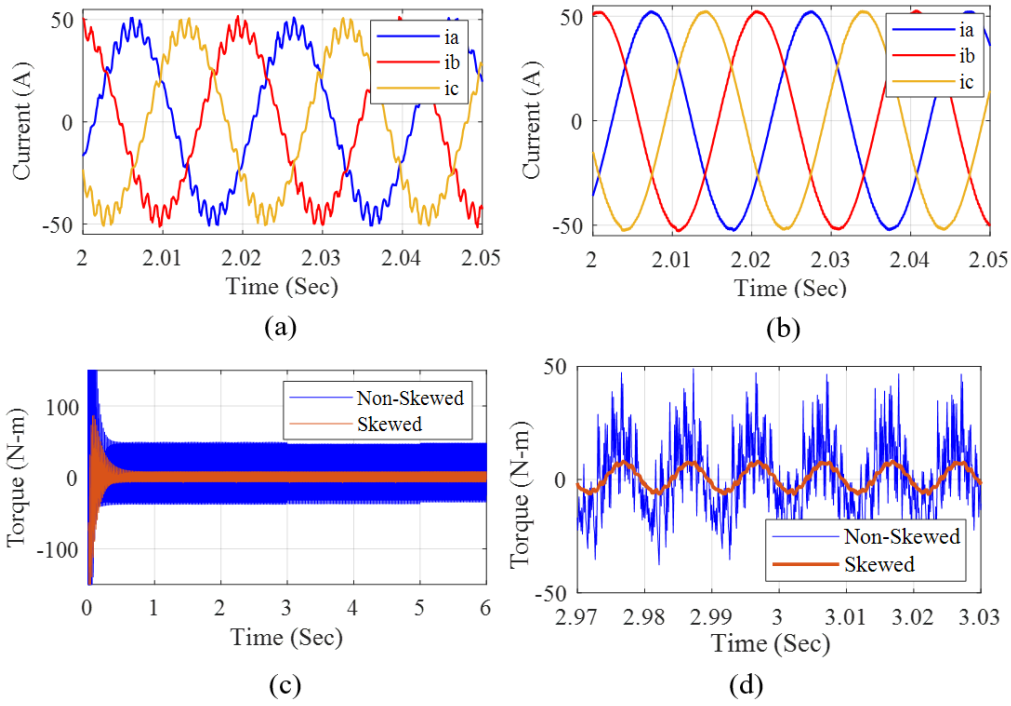

FIGURE 8. The stator currents with the rotor in (a) 2D without slot skew, (b) 3D with slot skew equal to one stator slot pitch, (c) the comparison of torque profile with and without rotor slot skews, (d) the zoomed comparison of torque profile with and without skews.

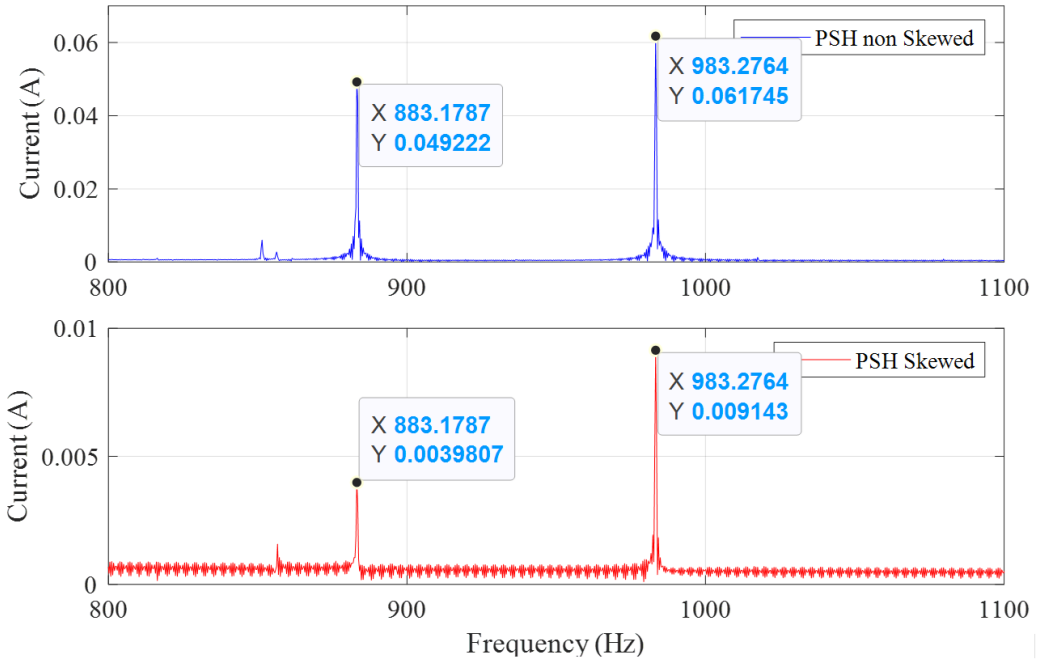

FIGURE 9. The development of PSH1 and PSH2 with and without slot skew in phase current.

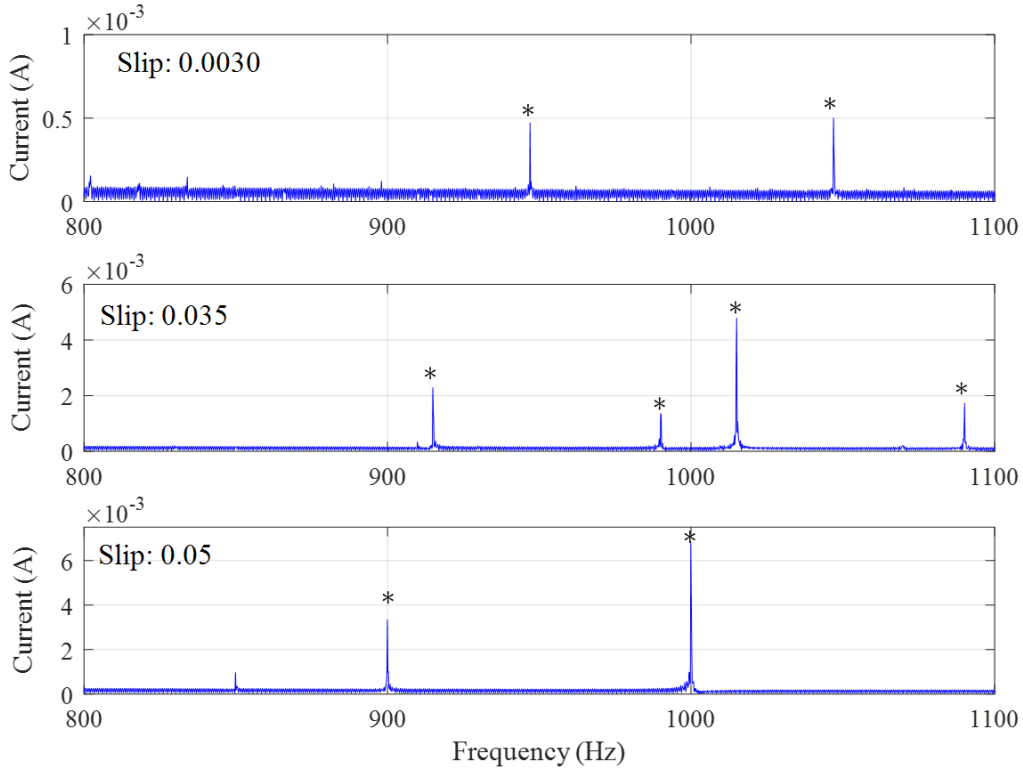

FIGURE 10. The development of PSH1 and PSH2 with skewed rotor bars while the PSH2 is present because the phase current is taken into consideration here.

slots changes the rotor winding function, which affects the PSH1 component while the PSH2 is very prominent here because the phase currents are considered. The frequency and amplitude of fundamental slotting harmonics are given in table 2.

In the line currents, the PSH2 components are cancelled out as shown in Figure (11). The development of PSH2 in the line current depends upon the non-linear behaviour of the magnetic material, local saturation on tooth tips, the fringing effects, any asymmetry in machine and supply unbalances.

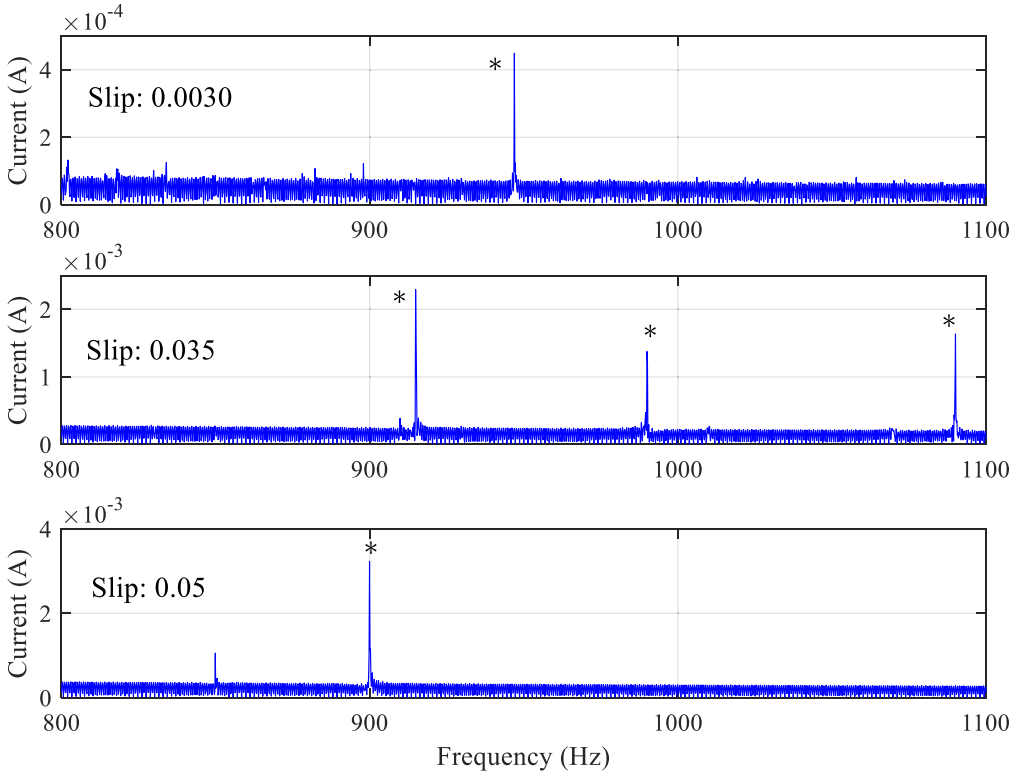

FIGURE 11. The development of PSH1 and cancellation of PSH2 with skewed rotor bars as the line currents are considered here while the supply is perfectly balanced.

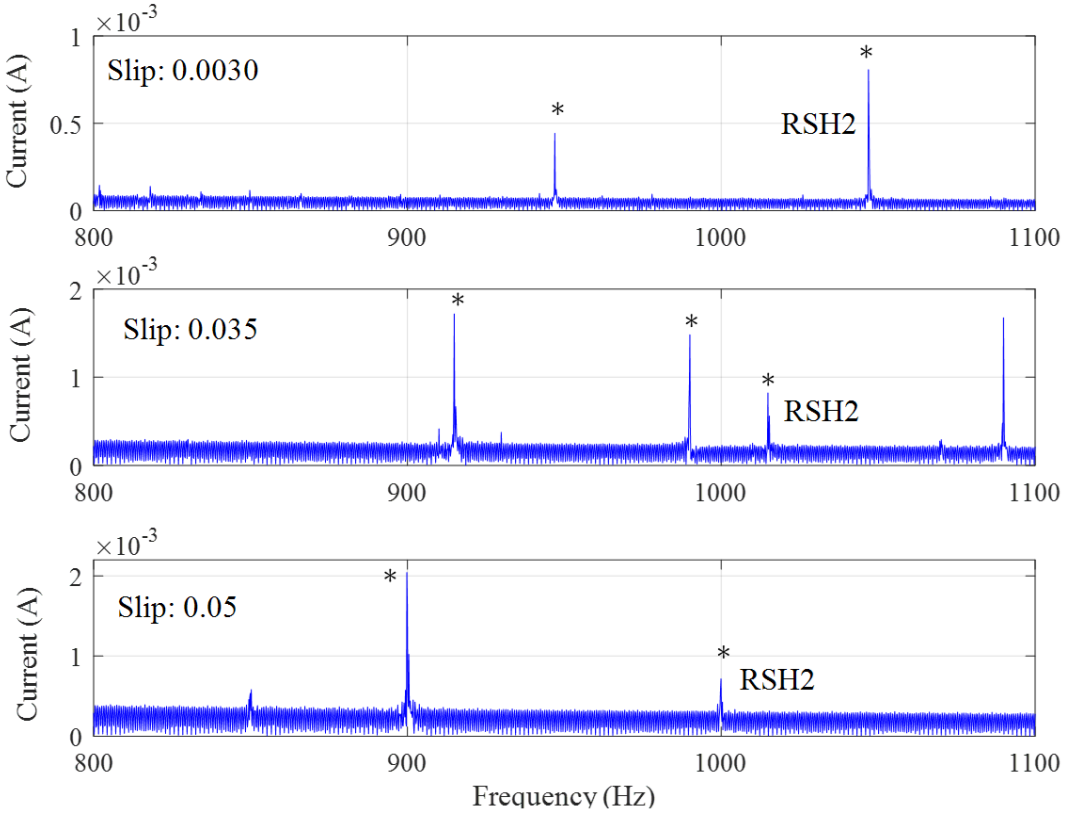

FIGURE 12. The development of PSH2 when the supply is made unbalanced according to the measured voltages from the supply side given in table 3.

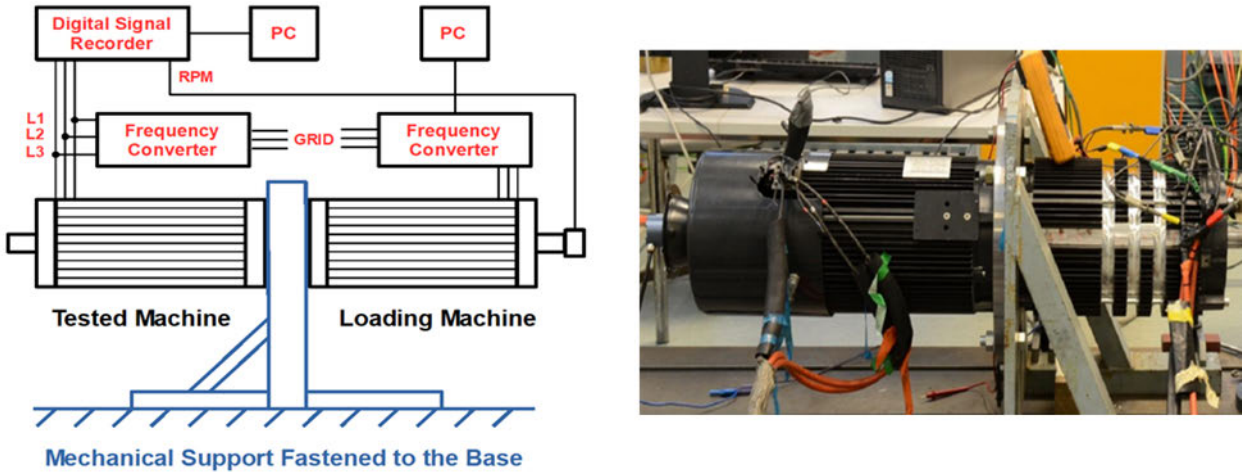

FIGURE 13. The experimental setup, block diagram (left), test rig (right).

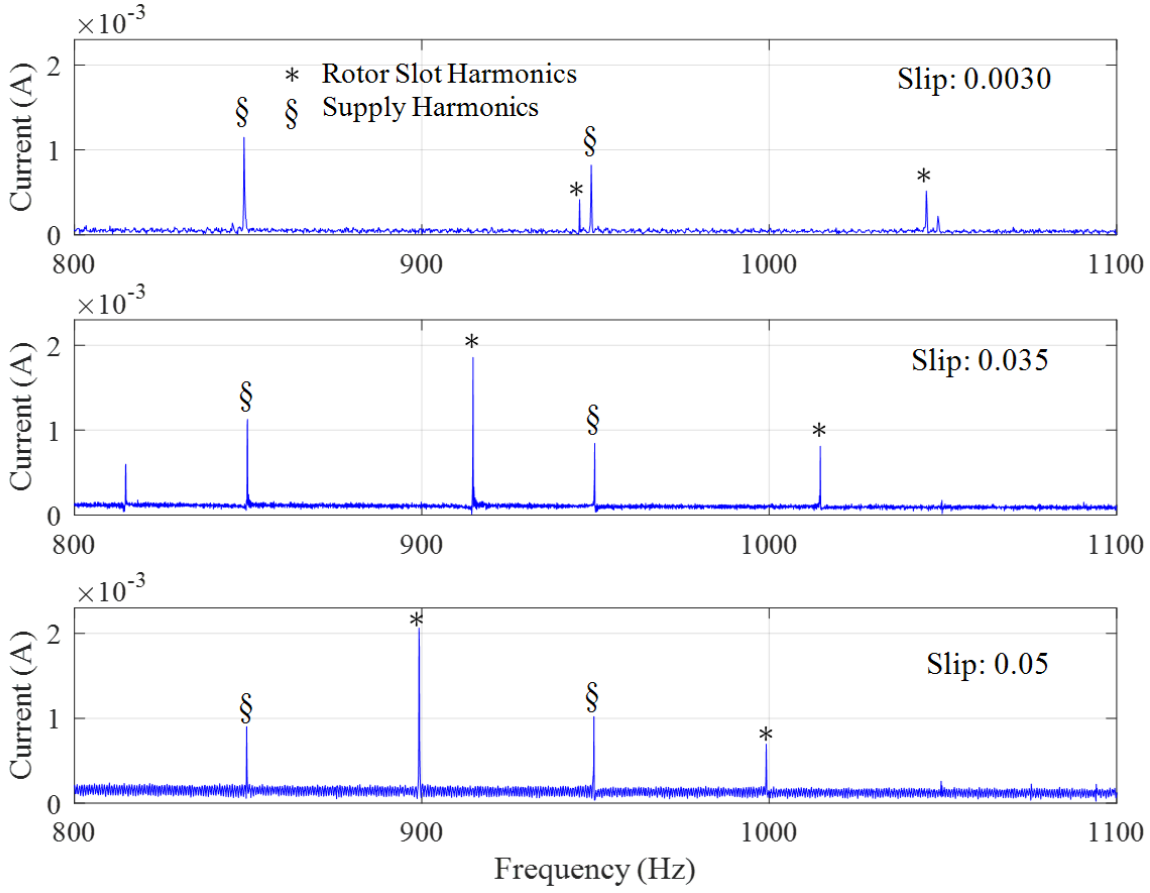

FIGURE 14. The PSH1 and PSH2 in practical measurements.

The tooth tip saturation and flux fringing effects can be simulated by reducing the height of stator and rotor slot openings however are neglected here. The development of the PSH2 component due to unbalanced supply is shown in Figure (12). For better understanding, the supply voltage in simulation is made the same as measured from the practical setup.

VII. PRACTICAL SETUP AND RESULTS

For experiments and measurements, a test rig is prepared, consisting of two identical motors coupled back to back as shown in Figure 13. One machine is under investigation while the other is acting as a load. Both machines are mounted on the same mechanical base and coupled through their shafts. The loading machine is fed through the inverters

TABLE 3. The supply based negative and zero sequence voltages.

slip	Va (V)	Vb (V)	Vc (V)	Zero seq. (V)	+ive seq. (V)	-ive seq. (V)
0.0030	191.747	190.256	190.522	0.557	188.711	0.557
0.035	192.436	191.155	187.878	1.233	188.241	1.235
0.05	194.418	189.331	191.131	1.533	188.765	1.533

TABLE 4. The development of PSH with skewed rotor in practical measurement.

Sr. No.	Parameter	Symbol	Value
1	Rated speed	N_r	1400 rpm@50 Hz
2	Rated power	P_r	18 kW@50 Hz
3	Connection	Y, Δ	Star (Y)
4	Power factor	cosφ	0.860
5	Number of poles	P	4
6	Number of rotor bars skewed	N_{rb}	40
7	Number of stator slots	Ns	48

TABLE 5. The development of PSH with skewed rotor in practical measurement.

Slip (Healthy)	RSH1 (Hz)	RSH2 (Hz)	RSH1 (A)	RSH2 (A)
0.0030	945.40	1045.20	0.00042	0.0005
0.035	914.76	1014.76	0.00189	0.0008
0.05	899.23	999.21	0.00233	0.0007

to improve its controllability for various load levels. Grid feeds the machine under investigation. The stator currents and voltages are measured using the Dewetron transient recorder. The measured signals' sampling frequency is 10 kHz, and the measurement time is 70 seconds, giving an excellent resolution of the frequency spectrum. The selection of appropriate sampling frequency also reduces the problems related to aliasing and mirror frequency components. The quality of supply voltage in the sense of negative and zero sequence components is presented in Table 3.

The negative sequence components result is flux rotating in opposite direction to the main flux. It results in the development of the RSH2 component with a corresponding increase in speed and torque ripples. The specifications of the machine under investigation are given in table 4.

The most prominent causes of current harmonics in induction machines are; supply, winding and inherent eccentricity based harmonics. Moreover, since both machine and its supply are not ideal, the factors such as, negative sequence currents generating reverse rotating field, the material local saturation points, flux fringing, the stator winding asymmetry, the skinning and proximity effects, the thermal effects on the resistance and leakage flux can also affect the slotting harmonics. As discussed earlier, most of these factors affect the PSH2 component quite significantly. This is why PSH2 is lower in amplitude than the PSH1 component, as described in Figure (14) and table 5.

The simulation results are in a very good agreement with the practical results. The RSH1 components obtained from simulation have almost same amplitude as the ones obtained from the practical measurements. However, a slight difference in RSH2 is due to neglecting the non-linear behaviour of magnetic material and local saturation of stator and rotor tooth tips. The material saturation can be included by using the B-H curve as a lookup table in the online section of the model, while local saturation can be incorporated by modulating the air gap and can be considered as future work in this domain.

VIII. CONCLUSION

A new approach for the modelling of a skewed rotor based squirrel cage induction motor has been presented in this paper. The conversion of a 2D continuous integration based winding function to a 3D discrete mean value equation, the definition of the air gap and winding functions using conditional analytical expressions and the inclusion of rotor slots skew are the crucial features of the proposed model.

For implementation, the model is divided into offline and online portions. All inductances and resistances are calculated as a function of rotor position in the offline portion, and results are saved in the 3D lookup table. The pre-saved results are then used in the online portion for the simulation of the performance parameters. By doing so, the offline calculations do not need to be calculated in the online portion, which decreases the simulation time considerably. As discussed in [25], the proposed model takes only three minutes per segment for the offline calculations while the online section takes only a few seconds to simulate the global parameters of the motor. This fact makes the model a good candidate for model-dependent condition monitoring algorithms. In comparison the FEM models can take several days to simulate the machine in 3D. In the light of the results and discussion following are the concluding remarks of the model.

- Since the model considers all design parameters as conditional analytical expressions, it is suitable for analyzing machine under various healthy and faulty scenarios. The fault cases may include broken rotor bars, broken end rings, static and dynamic eccentricity and stator short circuits.
- Since the model takes negligible simulation time compared to the corresponding FEM models, it is suitable for model-dependent fault diagnostic algorithms and drives where sensor-less speed estimation is required. The location of PSH components can be used for the estimation of slip without speed sensors.
- The transformation of the conventional integration based winding function formula to discrete mean value equation reduces the simulation time and computational complexity. Moreover, the integration constant related issues are also resolved.

- Unlike conventional winding function-based models where the harmonics are defined using Fourier series, the proposed model considers the design parameters and calculate the performance parameters. Thus, this approach reduces the problems of self-defined number, frequency and amplitude of current harmonics.
- *Most importantly*, the model can incorporate axial asymmetries in the machine, the rotor slot skews can be easily simulated. It is observed that with skewed rotor bars, the PSH has quite a different amplitude, which is impossible to study using conventional winding function based 2D models. The same is true in the case of 2D FEM models. Moreover, the 3D FEM models are computationally so intense that they do not remain suitable for model-dependent fault diagnostic algorithms and drives.
- It is observed that the PSH1 depends upon the winding configurations while PSH2 depends upon material, design and supply related asymmetries.
- The supply based negative sequence currents play a significant role in the development of PSH2 with the resultant increase in the speed and torque ripples.

As the model is suitable for the implementation of almost all faults and can simulate the results in negligible time as compared to the FEM models. With its increased applicability to incorporate axial asymmetry, it can be a very good choice for model-dependent fault diagnostic techniques.

REFERENCES

[1] B. Asad, T. Vaimann, A. Belahcen, A. Kallaste, A. Rassõlkin, and M. N. Iqbal, "Broken rotor bar fault detection of the grid and inverter-fed induction motor by effective attenuation of the fundamental component," *IET Electr. Power Appl.*, vol. 13, no. 12, pp. 2005–2014, Dec. 2019.

[2] M. Ojaghi, R. Aghmasheh, and M. Sabouri, "Model-based exact technique to identify type and degree of eccentricity faults in induction motors," *IET Electr. Power Appl.*, vol. 10, no. 8, pp. 706–713, Sep. 2016.

[3] G. Trejo-Caballero, H. Rostro-Gonzalez, R. de Jesus Romero-Troncoso, C. H. Garcia-Capulin, O. G. Ibarra-Manzano, J. G. Avina-Cervantes, and A. Garcia-Perez, "Multiple signal classification based on automatic order selection method for broken rotor bar detection in induction motors," *Elect. Eng.*, vol. 99, no. 3, pp. 987–996, 2017.

[4] R. H. C. Palácios, I. N. da Silva, A. Goedtel, and W. F. Godoy, "A novel multi-agent approach to identify faults in line connected three-phase induction motors," *Appl. Soft Comput.*, vol. 45, pp. 1–10, Aug. 2016.

[5] M. O. Mustafa, D. Varagnolo, G. Nikolakopoulos, and T. Gustafsson, "Detecting broken rotor bars in induction motors with model-based support vector classifiers," *Control Eng. Pract.*, vol. 52, pp. 15–23, Jul. 2016.

[6] V. Ghorbanian and J. Faiz, "A survey on time and frequency characteristics of induction motors with broken rotor bars in line-start and inverter-fed modes," *Mech. Syst. Signal Process.*, vols. 54–55, pp. 427–456, Mar. 2015.

[7] S. H. Saïd, M. F. Mimouni, F. M'Sahli, and M. Farza, "High gain observer based on-line rotor and stator resistances estimation for IMs," *Simul. Model. Pract. Theory*, vol. 19, no. 7, pp. 1518–1529, Aug. 2011.

[8] A. Sapena-Bano, F. Chinesta, M. Pineda-Sanchez, J. V. Aguado, D. Borzacchiello, and R. Puche-Panadero, "Induction machine model with finite element accuracy for condition monitoring running in real time using hardware in the loop system," *Int. J. Elect. Power Energy Syst.*, vol. 111, pp. 315–324, Oct. 2019.

[9] M. Jemli, H. B. Azza, and M. Gossa, "Real-time implementation of IRFOC for single-phase induction motor drive using dSpace DS 1104 control board," *Simul. Model. Pract. Theory*, vol. 17, no. 6, pp. 1071–1080, Jul. 2009.

[10] M. D. Prieto, G. Cirrincione, A. G. Espinosa, J. A. Ortega, and H. Henao, "Bearing fault detection by a novel condition-monitoring scheme based on statistical-time features and neural networks," *IEEE Trans. Ind. Electron.*, vol. 60, no. 8, pp. 3398–3407, Aug. 2013.

[11] V. Mukherjee, M. F. Far, F. Martin, and A. Belahcen, "Constrained algorithm for the selection of uneven snapshots in model order reduction of a bearingless motor," *IEEE Trans. Magn.*, vol. 53, no. 6, pp. 1–4, Jun. 2017.

[12] M. F. Far, F. Martin, A. Belahcen, P. Rasilo, and H. A. A. Awan, "Real-time control of an IPMSM using model order reduction," *IEEE Trans. Ind. Electron.*, vol. 68, no. 3, pp. 2005–2014, Mar. 2021.

[13] M. F. Far, F. Martin, A. Belahcen, L. Montier, and T. Henneron, "Orthogonal interpolation method for order reduction of a synchronous machine model," *IEEE Trans. Magn.*, vol. 54, no. 2, pp. 1–6, Feb. 2018.

[14] G. M. Joksimovic and J. Penman, "The detection of inter-turn short circuits in the stator windings of operating motors," *IEEE Trans. Ind. Electron.*, vol. 47, no. 5, pp. 1078–1084, Oct. 2000.

[15] J. Milimonfared, H. M. Kelk, S. Nandi, A. D. Minassians, and H. A. Toliyat, "A novel approach for broken-rotor-bar detection in cage induction motors," *IEEE Trans. Ind. Appl.*, vol. 35, no. 5, pp. 1000–1006, Sep. 1999.

[16] H. A. Toliyat and T. A. Lipo, "Transient analysis of cage induction machines under stator, rotor bar and end ring faults," *IEEE Trans. Energy Convers.*, vol. 10, no. 2, pp. 241–247, Jun. 1995.

[17] H. A. Toliyat, T. A. Lipo, and J. C. White, "Analysis of a concentrated winding induction machine for adjustable speed drive applications. I. Motor analysis," *IEEE Trans. Energy Convers.*, vol. 6, no. 4, pp. 679–683, Dec. 1991.

[18] H. A. Toliyat, T. A. Lipo, and J. C. White, "Analysis of a concentrated winding induction machine for adjustable speed drive applications. II. Motor design and performance," *IEEE Trans. Energy Convers.*, vol. 6, no. 4, pp. 684–692, Dec. 1991.

[19] A. M. El-Refaie, T. M. Jahns, and D. W. Novotny, "Analysis of surface permanent magnet machines with fractional-slot concentrated windings," *IEEE Trans. Energy Convers.*, vol. 21, no. 1, pp. 34–43, Mar. 2006.

[20] J. Faiz and I. Tabatabaei, "Extension of winding function theory for nonuniform air gap in electric machinery," *IEEE Trans. Magn.*, vol. 38, no. 6, pp. 3654–3657, Nov. 2002.

[21] S. Nandi, "Modeling of induction machines including stator and rotor slot effects," *IEEE Trans. Ind. Appl.*, vol. 40, no. 4, pp. 1058–1065, Jul. 2004.

[22] H. A. Toliyat, M. S. Arefeen, and A. G. Parlos, "A method for dynamic simulation of air-gap eccentricity in induction machines," *IEEE Trans. Ind. Appl.*, vol. 32, no. 4, pp. 910–918, Jul./Aug. 1996.

[23] J. Faiz and M. Ojaghi, "Unified winding function approach for dynamic simulation of different kinds of eccentricity faults in cage induction machines," *IET Electr. Power Appl.*, vol. 3, no. 5, p. 461, 2009.

[24] A. Marfoli, P. Bolognesi, L. Papini, and C. Gerada, "Mid-complexity circuital model of induction motor with rotor cage: A numerical resolution," in *Proc. 13th Int. Conf. Electr. Mach. (ICEM)*, Sep. 2018, pp. 277–283.

[25] B. Asad, T. Vaiman, A. Belahcen, A. Kallaste, A. Rassolkin, and M. N. Iqbal, "Modified winding function-based model of squirrel cage induction motor for fault diagnostics," *IET Electr. Power Appl.*, vol. 14, pp. 1–11, May 2020.

[26] M. Harir, A. Bendiabdellah, A. Chaouch, and N. Benouzza, "Modelling of induction motor including skew effect using MWFA for performance improvement," *Int. J. Elect. Comput. Eng.*, vol. 7, no. 12, pp. 1737–1743, Jan. 2014.

[27] J. M. Gojko, D. D. Momir, and O. B. Aleksandar, "Skew and linear rise of MMF across slot modelling-winding function approach," *IEEE Trans. Energy Convers.*, vol. 14, no. 3, pp. 315–320, Sep. 1999.

[28] S. Nandi, S. Ahmed, and H. A. Toliyat, "Detection of rotor slot and other eccentricity related harmonics in a three phase induction motor with different rotor cages," *IEEE Trans. Energy Convers.*, vol. 16, no. 3, pp. 253–260, Sep. 2001.

BILAL ASAD (Member, IEEE) was born in Pakistan, in 1986. He received the B.Sc. degree in electronics engineering from The Islamia University of Bahawalpur, in 2007, the M.Sc. degree in electrical engineering from the University of Engineering and Technology (UET) Lahore, Pakistan, in 2011, and the Ph.D. degree under cotutelle dual degree program from the Department of Electrical Power Engineering and Mechatronics, Tallinn University of Technology, Estonia, and the Department of Electrical Engineering and Automation, Aalto University, Espoo, Finland, in 2021. His research interests include signal processing, design, modeling, and fault diagnostics of electrical machines.

TOOMAS VAIMANN (Senior Member, IEEE) was born in Pärnu, Estonia, in 1984. He received the B.Sc., M.Sc., and Ph.D. degrees in electrical engineering from the Tallinn University of Technology, Estonia, in 2007, 2009, and 2014, respectively.

He is currently a Senior Researcher with the Department of Electrical Engineering, Tallinn University of Technology. Internationally, he has been a Postdoctoral Researcher with the Department of Electrical Engineering and Automation, Aalto University, Espoo, Finland, and works as a Visiting Professor with the Faculty of Control Systems and Robotics, ITMO University, St. Petersburg, Russia. He has been working in several companies as an Electrical Engineer. He is a member of Estonian Society of Moritz Hermann Jacobi and Estonian Society for Electrical Power Engineering. His research interest includes diagnostics of electrical machines.

ANOUAR BELAHCEN (Senior Member, IEEE) is currently a Professor in computational electromechanics with Aalto University, Finland. He has authored or coauthored more than 90 journal articles and several conference papers, many of them are the results of joint international cooperation, e.g., with French, German, Austrian, Spanish, Italian, Belgian, Portuguese, and Chinese research groups. His research interests include numerical modeling of electrical machines, magnetic materials characterization and modeling, coupled magneto-mechanical problems, magnetic forces and magnetostriction, iron losses, and fault diagnostics of electrical machines. He is a Senior Member of the IEEE Society and a member of the first Board (AdCom) of the ICEM NPO, which manages the ICEM conferences and a member of the ICS board, which manages the COMPUMAG conference. He is a regular participant in the major conferences in his field, including COMPUMAG, CEFC, ICEM and SDEMPED, where he has been acting as the Session Chair and Track Chair. At the university level, he is the Deputy Head of his department and the Director of the Master's Programme in automation and electrical engineering with more than 100 students entering the programme each year. He is also the Deputy Head of the Quality of Education Committee (QEC), responsible for the assessment of teaching and learning. Besides his work at Aalto University, he has been working as an Invited Professor with the Tallinn University of Technology, Estonia, since 2011, where he has been teaching subject related to electrical machines and supervising Ph.D. and postdoctoral researchers.

ANTS KALLASTE (Senior Member, IEEE) was born in Pärnu, Estonia, in 1980. He received the B.Sc., M.Sc., and Ph.D. degrees in electrical engineering from the Tallinn University of Technology, Estonia, in 2004, 2006, and 2013, respectively. He is currently a Professor in electrical machines with the Department of Electrical Power Engineering and Mechatronics, Tallinn University of Technology. In addition, he is holding the position of the Head of Chair of the Electrical Machines Research Group. He is a member of the Estonian Society of Moritz Hermann Jacobi.

ANTON RASSOLKIN (Senior Member, IEEE) was born in Tallinn, Estonia, in 1985. He received the B.Sc., M.Sc., and Ph.D. degrees in electric drives and power electronics from the Tallinn University of Technology, Estonia, in 2008, 2010, and 2014, respectively, and the Dipl.-Ing. degree in automatic from the University of Applied Science Giessen-Friedberg, Germany, in 2010.

HUYNH VAN KHANG (Senior Member, IEEE) received the B.Sc. degree in electrical engineering from the Ho Chi Minh City University of Technology, Ho Chi Minh City, Vietnam, in 2002, the M.Sc. degree in electrical engineering from Pusan National University, Busan, South Korea, in 2008, and the D.Sc. (Tech.) degree in electrical engineering from Aalto University, Espoo, Finland, in 2012.

He was an Associate Professor in electrical power engineering with the University of Agder, Grimstad, Norway, from 2013 to 2019, where he is currently a Professor with the Department of Engineering Sciences. His research interests include electrical machines, condition-based maintenance, and applied power electronics.

PAYAM SHAMS GHAHFAROKHI (Member, IEEE) was born in Iran, in 1986. He received the B.Sc. degree in electrical power engineering from IAUN, Iran, in 2010, the M.Sc. degree in electrical power engineering from Newcastle University, U.K., in 2011, and the Ph.D. degree in electrical engineering and machines from the Tallinn University of Technology, Estonia, in 2019. He is currently a Senior Researcher and a Postdoctoral Researcher with the Department of Electrical Machines and Apparatus, Riga Technical University, Latvia. His research interests include electromagnetic design and thermal management of PM and synchronous reluctance electrical machines.

MUHAMMAD U. NASEER (Member, IEEE) was born in Pakistan, in 1990. He received the B.Sc. degree in electrical engineering from the Islamia University of Bahawalpur, in 2011, and the M.Sc. degree from the University of Engineering and Technology (UET), Lahore, Pakistan. He is currently pursuing the Ph.D. degree with the Tallinn University of Technology. His research interests include electrical machines modeling, design, and optimization.

MUHAMMAD N. IQBAL (Member, IEEE) was born in Pakistan, in 1988. He received the B.Sc. degree in electronics engineering from the Islamia University of Bahawalpur, in 2008, the M.S. degree from the University of New South Wales, Australia, and the Ph.D. degree from the Tallinn University of Technology, in 2021. His research interests include energy consumption modeling and power quality.